Remeasuring HEWL pKa values by NMR spectroscopy: Methods, analysis, accuracy, and implications for theoretical pKa calculations

ARTICLE *in* PROTEINS STRUCTURE FUNCTION AND BIOINFORMATICS · MARCH 2011

Impact Factor: 2.63 · DOI: 10.1002/prot.22886 · Source: PubMed

10 AUTHORS, INCLUDING:

Damien Farrell
University College Dublin
17 PUBLICATIONS **186** CITATIONS
SEE PROFILE

Fergal O'Meara
University College Dublin
9 PUBLICATIONS **80** CITATIONS
SEE PROFILE

Kaare Teilum
University of Copenhagen
38 PUBLICATIONS **1,378** CITATIONS
SEE PROFILE

Jens Erik Nielsen
Novozymes
67 PUBLICATIONS **4,396** CITATIONS
SEE PROFILE

PROTEINS
STRUCTURE ■ FUNCTION ■ BIOINFORMATICS

Remeasuring HEWL pK_a values by NMR spectroscopy: Methods, analysis, accuracy, and implications for theoretical pK_a calculations

Helen Webb,[1] Barbara Mary Tynan-Connolly,[1] Gregory M. Lee,[2] Damien Farrell,[1] Fergal O'Meara,[1] Chresten R. Søndergaard,[1] Kaare Teilum,[3] Chandralal Hewage,[4] Lawrence P. McIntosh,[2] and Jens Erik Nielsen[1]*

[1] School of Biomolecular and Biomedical Science, Centre for Synthesis and Chemical Biology, UCD Conway Institute, University College Dublin, Belfield, Dublin 4, Ireland

[2] Department of Biochemistry and Molecular Biology, Department of Chemistry, and the Michael Smith Laboratories, Life Sciences Centre, 2350 Health Sciences Mall, The University of British Columbia, Vancouver, British Columbia, Canada, V6T 1Z3

[3] Structural Biology and NMR Laboratory, Department of Biology, University of Copenhagen, DK-2200 Copenhagen N, Denmark

[4] School of Biomolecular and Biomedical Science, Centre for Synthesis and Chemical Biology, SEC Strategic Research Cluster, UCD Conway Institute, University College Dublin, Belfield, Dublin 4, Ireland

ABSTRACT

Site-specific pK_a values measured by NMR spectroscopy provide essential information on protein electrostatics, the pH-dependence of protein structure, dynamics and function, and constitute an important benchmark for protein pK_a calculation algorithms. Titration curves can be measured by tracking the NMR chemical shifts of several reporter nuclei versus sample pH. However, careful analysis of these curves is needed to extract residue-specific pK_a values since pH-dependent chemical shift changes can arise from many sources, including through-bond inductive effects, through-space electric field effects, and conformational changes. We have re-measured titration curves for all carboxylates and His 15 in Hen Egg White Lysozyme (HEWL) by recording the pH-dependent chemical shifts of all backbone amide nitrogens and protons, Asp/Glu side chain protons and carboxyl carbons, and imidazole protonated carbons and protons in this protein. We extracted pK_a values from the resulting titration curves using standard fitting methods, and compared these values to each other, and with those measured previously by ^{1}H NMR (Bartik et al., Biophys J 1994;66:1180–1184). This analysis gives insights into the true accuracy associated with experimentally measured pK_a values. We find that apparent pK_a values frequently differ by 0.5–1.0 units depending upon the nuclei monitored, and that larger differences occasionally can be observed. The variation in measured pK_a values, which reflects the difficulty in fitting and assigning pH-dependent chemical shifts to specific ionization equilibria, has significant implications for the experimental procedures used for measuring protein pK_a values, for the benchmarking of protein pK_a calculation algorithms, and for the understanding of protein electrostatics in general.

Proteins 2011; 79:685–702.

Key words: protein pK_a values; NMR monitored pH titration; pK_a calculations; chemical shift.

INTRODUCTION

The pH-dependence of protein enzymatic activity, structural stability and dynamics is governed by the acid dissociation equilibria (or pK_a values) of the ionizable groups in the protein. The perturbations of protein pK_a values from their corresponding values in a random coil

Additional Supporting Information may be found in the online version of this article.

Grant sponsor: SFI PIYR Award; Grant number: 04/YI1/M537; Grant sponsor: SFI Research Frontiers Programme Award; Grant number: 08/RFP/BIC1140; Grant sponsor: Danish Natural Science Research Council; Grant number: 272-060251; Grant sponsors: Natural Sciences and Engineering Research Council of Canada; Canadian Institutes for Health Research; Canadian Foundation for Innovation; British Columbia Knowledge Development Fund; UBC Blusson Fund; Michael Smith Foundation for Health Research (MSFHR).

Gregory M. Lee's current address is Department of Pharmaceutical Chemistry, University of California, Mission Bay, Genentech Hall, 600 16th St, Box 2280, San Francisco, California 94143-2280

*Correspondence to: Jens Erik Nielsen, School of Biomolecular and Biomedical Science, Centre for Synthesis and Chemical Biology, UCD Conway Institute, University College Dublin, Belfield, Dublin 4, Ireland. E-mail: jens.nielsen@ucd.ie

Received 27 January 2010; Revised 24 August 2010; Accepted 3 September 2010
Published online 17 September 2010 in Wiley Online Library (wileyonlinelibrary. com).
DOI: 10.1002/prot.22886

polypeptide serve as highly sensitive probes of the electric field and local dielectric properties within proteins, and the experimental and theoretical study of protein pK_a values and protein electrostatics in general therefore continues to receive significant interest.[1]

The interest in protein titration curves and protein pK_a values stems from a desire to understand the energetics, and in particular the electrostatics, of proteins and protein complexes. Structure-based energy calculation methods play a large role in protein engineering and design,[2,3] drug design,[4] and in developing a better understanding of biomolecules through molecular simulations.[5] Present methods for predicting pK_a values from a protein structure fall into several categories: Poisson-Boltzmann based methods,[6–11] knowledge-based methods[12,13] and molecular dynamics-based methods.[14–16] Common to all of these is that their performance is benchmarked and optimized against experimentally measured pK_a values. Improvements in our understanding of protein electrostatics therefore necessitate a better understanding of the accuracy of experimentally measured pK_a values.

NMR-monitored pH-titrations are the method of choice for measuring site-specific pK_a values of ionizable moieties in proteins. Experimentally determined titration curves are typically fit to equations describing one or more sequential acid dissociation equilibria, or to equations modeling two or more coupled titrations[17] to extract the apparent pK_a values of titratable groups in a protein. Such analyses of titration curves have yielded valuable data for understanding the effects of the protein environment on the ionization equilibria of titratable groups, and has allowed for the analysis of large sets of measured pK_a values[18–20] using theoretical methods.[13,21] Recently, global analysis of tightly coupled systems of titratable groups has been performed,[22] and analyses probing the electric field in proteins[23] and protein conformational change[24,25] have pointed to exciting new ways of analyzing NMR pH-titration curves.

Finally, it should be noted that some titration curves are irregular and cannot be described by a single pK_a value. Such titration curves can be slightly "flattened" and are often fitted by the modified Hill equation (see later), or they can be highly irregular[26,27] and thus necessitate the application of specialized fitting procedures.[22] In these cases, which often reflect very interesting coupled ionization equilibria, one must analyze the entire titration curves, rather than describing them with single pK_a values. Although we do not address this problem in the present work, it is important to keep the existence of such titration curves in mind when assessing the accuracy and significance of pK_a values reported in literature and databases.

Measuring pH-titration curves using NMR

Researchers exploit the unique sensitivity of the NMR chemical shift to measure residue-specific protein titration curves. Typically 1D or 2D spectra are acquired as a function of sample pH over a range of interest and the chemical shifts for nuclei with resolved and assigned signals are analyzed. The change in solution pH leads to a change in the charge of ionizable groups, and the chemical shifts of nearby nuclei are influenced via through-bond inductive effects, through-space electrostatic field effects, or via conformational changes. Plots of the NMR chemical shift versus pH obtained in this way thus often show typical Henderson-Hasselbalch (HH) titration curves, indicative of a single dominant acid dissociation equilibrium. These HH curves are interpreted as reporting the ionization states of the titratable groups in the protein, and they can therefore easily be fitted to yield apparent pK_a values for the titratable groups in question.

Although it is possible to observe unambiguously the charge state of ionizable groups by directly monitoring labile titratable protons by NMR spectroscopy,[28,29] this requires that these protons are significantly protected by burial or hydrogen bonding from rapid exchange with water. However, since most titrating protons are unobservable due to fast exchange, we are usually limited to measuring the pH-dependent chemical shifts of the nearby nonlabile ^{1}H, ^{15}N, or ^{13}C nuclei from which the charge states and pK_a values of ionizable groups can be inferred. The exquisite sensitivity of the NMR chemical shift to changes in structure and changes in the electric field[23,30] means that a given titration can be observed indirectly via a large number of surrounding "reporter" nuclei. On one hand, this allows multiple measurements of the same ionization event. However, unambiguously assigning even simple titration curves to specific moieties is often difficult as electric field effects can be observed at distances well over 20 Å and similarly, structural and conformational changes may be propagated over large distances depending on the structural plasticity of the protein.[24] The fact that ionizations can be observed via the pH-dependence of the chemical shift of neighboring and distant nuclei also means that a given nucleus may track two or more titration events, thus further complicating the extraction of pK_a values and the assignment of these values to specific residues, as discussed below.

Spectral assignment

It is important to note that the correct measurement of site-specific pK_a values relies on a careful assignment of NMR peaks to the correct atoms/nuclei in the protein. An incorrect peak assignment will lead to pK_a values being assigned to wrong residues thus rendering the experiment meaningless. Tracking individual NMR peaks as the pH changes is another challenge since peaks often can be seen to move in nonlinear paths. This causes difficulty in resolving the identity of peaks when the paths of two or more peaks cross during the NMR pH-titration experiment. This problem becomes more significant for poor spectra and when the pH is changed in larger steps.

It is therefore advisable to perform experiments that check the NMR peak assignment at low, intermediate, and high pH values to confirm that the relevant peaks have been tracked correctly.

Fitting NMR pH-titration curves

Once the required titration curves have been obtained, pK_a values are typically extracted using non-linear fits to equations relating changes in population-weighted chemical shift (δ_{obs}) to changes in protonation state. Well-defined curves displaying single titrations in the fast exchange limit are typically fit to an expression such as:

$$\delta_{obs} = \frac{\Delta\delta_a}{1 + 10^{pH-pK_a}} + \delta_{offset} \quad (1)$$

where $\Delta\delta_a$ corresponds to the difference in chemical shift of a nucleus resulting from the nucleus in the presence of the protonated form of that moiety. Equation (1) is equivalent to chemical shifts weighted by the Henderson-Hasselbalch (HH) equation:

$$pH = pK_a + \log[A^-]/[HA] \quad (2)$$

If two or more titratable groups influence the monitored nuclei, then the observed titration curves can be non-HH shaped. This is a result of the chemical shift of the nuclei sensing more than one titrational event. These multi-phasic titration curves can be fit to equations such as:

$$\delta_{obs} = \frac{\Delta\delta_a}{1 + 10^{pH-pK_{a1}}} + \frac{\Delta\delta_b}{1 + 10^{pH-pK_{a2}}} + \frac{\Delta\delta_c}{1 + 10^{pH-pK_{a3}}} + \delta_{offset} \quad (3)$$

where, $\Delta\delta_a$, $\Delta\delta_b$, and $\Delta\delta_c$ refer to the chemical shift changes associated with the titrations described by pK_a values 1–3. Note that this expression describes sequential rather than coupled ionization equilibria.

Irregular and multiphasic titration curves can also be fit to higher-order equations such as the modified version of the Hill equation [Eq. (4)], or equations that model coupled ionization equilibria [Eq. (5)].

The modified Hill equation[31] is given by:

$$\delta_{obs} = \frac{\Delta\delta_a}{1 + 10^{n(pH-pK_a)}} + \delta_{offset} \quad (4)$$

where $\Delta\delta_a$ refers to the chemical shift change associated with the titration described by the pK_a value, δ_{offset} is the chemical shift of the fully protonated species, and n is the phenomological Hill coefficient.

Coupled ionization equilibria in a two-group system are typically modeled by equation 5[32]:

$$\delta_{obs} = \frac{\Delta\delta_a(1 + 10^{pH-pK_{a4}})}{1 + 10^{pK_{a2}-pH} + 10^{pK_{a2}-pK_{a1}} + 10^{pH-pK_{a4}}} + \delta_{offset} \quad (5)$$

where $\Delta\delta_a$ refers to the chemical shift change associated with the full deprotonation of the group governed by the microscopic pK_{a2} and pK_{a4} values (i.e., ionization equilibria with the partner group in a neutral or charged state, respectively). pK_{a1} and pK_{a3} refer to the ionizations of the other group in the system (constrained by the linkage $pK_{a2} + pK_{a4} = pK_{a1} + pK_{a3}$), and δ_{offset} is the chemical shift of the fully protonated species. Coupled ionization equilibria can also be modeled by methods based on statistical mechanics[22,27] that may allow for the extraction of physical quantities from the perturbed titration curves.

Ghost titrations

A fundamental problem in interpreting NMR pH-titration curves is to identify the titration that gives rise to an observed chemical shift change. Generally the chemical shift of a nucleus is dominated by the protonation state of the nearest titratable group, although there are significant deviations from this rule in the case of atoms connected to a highly polarizable bond (e.g., the peptide bond), and in the case of titrational events causing structural perturbations.

In the following we define a "ghost titration" as a titration observed in the chemical shift of a nucleus in residue A that results from an ionization event occurring in a different amino acid residue B. An example of an NMR titration curve reporting ghost titrations is provided in Figure 1, where a comparison of NMR pH-titration curves from two mutants reveals that the biphasic titration reported by the chemical shift of the backbone amide nitrogen of Asp48 in HEWL reports the ionization equilibria of Glu35 and Asp52 rather than that of Asp48 itself. Ghost titrations will often be superimposed on "true" (or "self") titrations (i.e., titrations originating from within the residue being monitored) or on other ghost titrations. If the chemical titration responsible for inducing the ghost titrations follows the classic Henderson-Hasselbalch (HH) equation, then the ghost titrations must be fit with variations of Eq. (3). In cases where a ghost-inducing residue titrates with a non-HH behavior the analysis must involve combinations of Eqs. (3) and (5), possibly coupled with statistical mechanical methods.

Choosing the correct model

A scientist wishing to determine pK_a values from NMR-monitored pH-titration curves is forced to choose a fitting equation/model. This choice of model implicitly

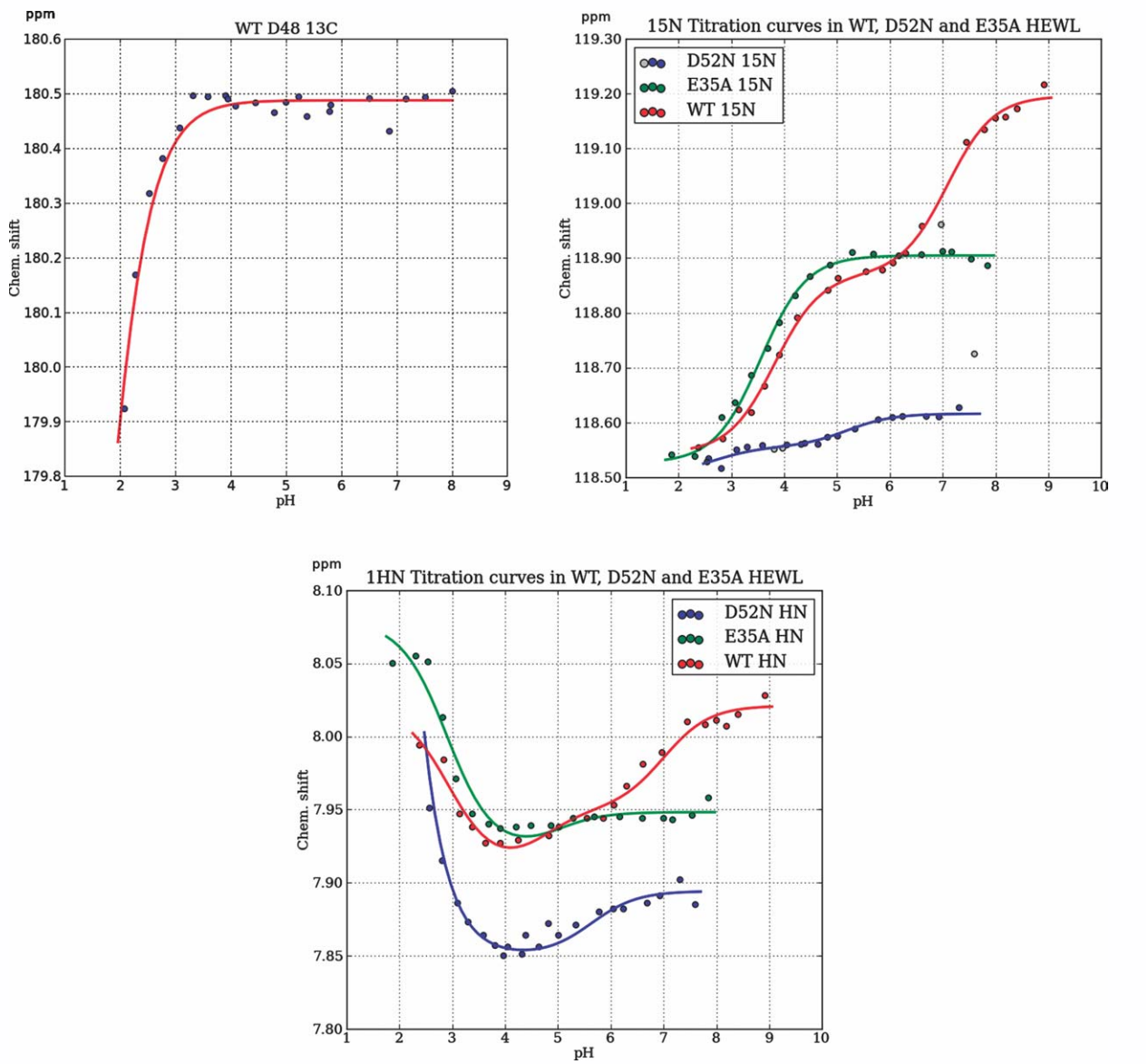

Figure 1

$^{13}C^{\gamma}$,^{15}N and ^{1}H titration curves of D48 in WT, D52N and E35A HEWL. Left top: the monophasic titration curve observed by monitoring the chemical shift perturbation of the side chain $^{13}C^{\gamma}$ of Asp48 in WT HEWL, which can be fit using a pK_a value of 1.6 ± 0.06 (only the curve for one of the C^{γ}-H^{β} cross peaks are shown). Right top: the biphasic titration curves observed by monitoring the chemical shift perturbations of the amide ^{15}N of Asp48 in WT (red), D52N (blue) and E35A (green) HEWL. Bottom: the biphasic titration curves observed by monitoring the chemical shift perturbations of the amide $^{1}H^{N}$ of Asp48 in WT (red), D52N (blue), and E35A (green) HEWL. It is clear that the WT titration curve must be fit using 2 pK_a values. Based on D52N and E35A mutants, the titrations observed by the amide nitrogen of Asp48 predominantly report the titrations of Asp52 and Glu35, rather than that of its own carboxyl. Whereas the mutation of Glu35 clearly identifies the titration of Glu35, the effect of the D52N mutation is more complicated to analyze due to the strong interaction between Glu35 and Asp52, and due to the changes in the local structure around Asp48 that D52N introduces. The proton titration curves display a more complex behavior, but still allows for the identification of Glu35 being responsible for the titration with a high pK_a value. Figure produced using EKIN.[33]

assumes a specific physical behavior for the titratable group in question. For example, if the HH equation [Eqs. (1) and (2)] is applied, it implies that the titration in question can be modeled perfectly by a two-state mechanism corresponding to a single ionization equilibrium. Slightly perturbed titration curves are often fit with the modified Hill equation, thereby casting deviations from a single ionization equilibrium as an apparent Hill parameter *n*. However, interpreting the Hill parameter in terms of specific electrostatic or structural interactions is difficult.

In the case of highly perturbed, multiphasic titration curves, Eqs. (3), (5) and the statistical mechanical methods can be used. However, Eqs. (3) and (5) are mathe-

matically interconvertable and differ only whether one chooses to interpret the fit pK_a values and chemical shift changes as describing sequential macroscopic or coupled microscopic ionization equilibria.[32] Similarly the statistical mechanical methods[22,27] can reproduce any titration curve shape with enough free parameters, although some guidance can be taken from assessing whether the extracted electrostatic interaction energies are realistic. Thus, equally good fits can be obtained with multiple models, yet the choice of model has implications for the physical interpretation of the extracted pK_a values. In the case of irregular titration curves, much information is lost when titrations are simply described by apparent pK_a values and Hill constants.

Other problems arise in the fitting of chemical shift titration curves that track two or more overlapping titrations with similar pK_a values (i.e., within 1 pK_a unit). Such titration curves often cannot be fit robustly to Eq. (3).

Although the choice of fitting model can sometimes be guided by the use of statistical treatments such as an F-test,[18] it is necessary to visually inspect titration curves and use additional information to ensure that the appropriate fitting model is chosen. Such information includes consideration of the protein structure as well as the argument that interacting ionizable residues should share common fit pK_a values. The process of choosing the appropriate fitting model thus essentially comes down to a subjective choice, and in the present work we employ conservative human judgment when fitting the titration curves to arrive at a measure of the true experimental error of pK_a values.

Obtaining a realistic error estimate of fitted pK_a values

Determination of protein pK_a values is the result of a two-step process as outlined above: (1) an NMR titration experiment and (2) a fitting procedure. Both the NMR experiment and the fitting procedure are conducted under certain assumptions, and these influence the resulting pK_a values. In addition to assumptions regarding the validity of the theoretical model and general assumptions about the NMR experiments (i.e., constant ionic strength, a single protein conformation and ideal solution behavior), the titration curves are also influenced by the experimental uncertainty.

The measurement of pH constitutes the largest source of systematic and random experimental error. Even assuming that care has been taken to control temperature, isotope effects, solution conditions and so on, pH values in most NMR titration experiments are realistically only accurate to within ± 0.1 units, although it should be possible to achieve higher accuracy with improved experimental protocols and equipment. In addition the identification and tracking of NMR peaks comes with an experimental uncertainty that increases for broad, poorly defined and overlapping peaks. To account for this fact, the robustness of the pK_a value fits can be tested by randomly perturbing individual pH data points by ± 0.1 units and the chemical shift components by reasonable spectral-dependent values, such as: ± 0.02 ppm (^{1}H), ± 0.05 ppm (^{15}N), and ± 0.2 ppm (^{13}C). This type of Monte Carlo error analysis gives a good estimate of the error inherent in pK_a values and the limiting chemical shifts obtained from a titration curve. However, the analysis does not include an estimate of how much the fitted pK_a value is influenced by the choice of nuclei being tracked, nor does the analysis investigate the impact of choosing a specific model for the fitting procedure. As a result, the experimental errors on measured pK_a values are generally not true estimates of accuracy, but merely reflect the precision associated with extracting an apparent pK_a value from a given titration curve. This fact has been acknowledged earlier,[34–36] and in the NMR community it is well-known that nuclei can sense several titrations as evidenced by comments on this issue in almost every paper that reports NMR-measured pK_a values. However only a handful of measurements are available showing the true accuracy of ^{13}C-measured pK_a values[37–39] (see Supporting Information Table SI4 and later), and no systematic studies are, to our knowledge, available on the reliability of pK_a values measured by other NMR experiments.

Examining the accuracy of pK_a values

In the present study, we study the differences in pK_a values determined from various types of NMR pH-titration experiments. Specifically, we remeasured the carboxyl and imidazole pK_a values of Hen Egg White Lysozyme (HEWL) by tracking the chemical shifts of several different nuclei. We furthermore reanalyzed the NMR titration curves of Bartik et al.[40] and compare the pK_a values determined in this article to those reported in literature during the last four decades (Table I).

It is important to note that we do not explicitly determine the experimental error of pK_a values measured using a given technique. Such measurements have been performed by several groups by performing repeat titrations on the same protein[37–39] (see Supporting Information Table SI4) and have mostly yielded very low values for the error on ^{13}C-measured pK_a values (0.01–0.04 pK_a units). Although a case can be made for extending such studies to observe the variation in pK_a values when different research groups perform the sample preparation and titration experiment, we focus on the problem of estimating the variation in pK_a values when measured with different NMR-based techniques. In doing so, we assume that pK_a values measured by observing ^{13}C chemical shifts close to the ionizable moiety give the most accurate measure of the true pK_a value of that moiety.

Table I
HEWL pK_a Values Available in Literature and Those Measured in This Study

Titratable group	Bartik *et al.*[40]	Others	Webb *et al.*	Max. difference
N-term		7.9[41 a]		—
Lys1		10.13 ± 0.03[42]		—
Arg5				—
Glu7	2.85 ± 0.25	2.6[43]	2.6 ± 0.2	0.25
Lys13		9.88 ± 0.03[42]		—
Arg14				—
His15	5.36 ± 0.07	5.8[43]	5.5 ± 0.2	0.44
Asp18	2.66 ± 0.08		2.8 ± 0.3	0.14
Tyr20		10.3[41]		—
Arg21				—
Tyr23		9.8[44]		—
Lys33		9.92 ± 0.05[42]		—
Glu35	6.20 ± 0.10	6.1,[45,46] 5.9[47 b]	6.1 ± 0.4	0.2
Arg45				—
Asp48	<2.5		1.4 ± 0.2	—
Asp52	3.68 ± 0.08	3.4,[45,46] 4.5[47 b]	3.6 ± 0.3	0.9
Tyr53		12.1[41]		—
Arg61				—
Asp66	<2.0	1.6[48]	1.2 ± 0.2	0.4
Arg68				—
Arg73				—
Asp87	2.07 ± 0.15		2.2 ± 0.1	0.13
Lys96		10.2 ± 0.08[42]		—
Lys97		9.64 ± 0.03[42]		—
Asp101	4.09 ± 0.07	4.5[45]	4.5 ± 0.1	0.41
Arg112				—
Arg114				—
Lys116		9.76 ± 0.03[42]		—
Asp119	3.20 ± 0.09		3.5 ± 0.3	0.3
Arg125				—
Arg128				—
C-term	2.75 ± 0.02	3.1[43]	2.7 ± 0.2/ 3.9 ± 0.1	1.15

The last column shows the largest difference observed for the pK_a value of a given residue.
[a]Estimated from global titration curves.[41]
[b]These studies report both microscopic and macroscopic pK_a values as well as the dependence of the pK_a values on ionic strength.

We base this assumption on the fact that the immediate chemical environment has the largest effect on the NMR chemical shift, and continue to note that pK_a values measured from the chemical shifts of $^{13}C^{\gamma}$ (Asp), $^{13}C^{\delta}$ (Glu), and imidazole ring carbon atoms for His are more reliable since they generally produce fewer and more regular titrations associated with larger chemical shift changes (see later). Consequently, in this paper, we assess the accuracy of pK_a values measured using other techniques by comparing them to ^{13}C-measured pK_a values.

Specifically we show that the apparent pK_a values of HEWL originating from measurements of the chemical shift at H^{β} protons and from the backbone amide protons and nitrogen are significantly different from those measured at ^{13}C atoms close to the titratable moiety.

In particular, we find the apparent pK_a values from backbone amide protons and nitrogens to be very unreliable and display differences to ^{13}C-measured pK_a values of up to 1.0 unit.

This results from their sensitivity to ghost titrations and generally smaller shift changes than observed with carboxyl or imidazole nuclei. We furthermore highlight two cases showing that even the accuracy of ^{13}C-measured pK_a values can be more ambiguous than reported in literature, and we discuss the consequences this has for the reliability of published pK_a values.

Finally, we discuss the implications of our findings for the benchmarking of protein pK_a calculation software and for the understanding of protein electrostatics in general.

MATERIALS AND METHODS

Sample preparation (WT HEWL and HEWL mutants)

The expression of uniformly isotopic-labeled WT HEWL (^{15}N and $^{13}C/^{15}N$) was performed using 5 g $^{13}C_6$-glucose, 10 mL ^{13}C-methanol, and 10 g $(^{15}NH_4)_2SO_4$ (CKGas Limited) in a 2 L Bioflo 110 fermentor (New Brunswick) using a P. Pastoris hewl expression system generously made available to us by Prof. J.F. Kirsch. Separate samples for the uniformly $^{13}C/^{15}N$ (WT HEWL only) and ^{15}N (WT HEWL and HEWL mutants, E7Q, H15A, D18N, E35A, D48N, D52N, D66N, D101N, and D119N) were dialyzed into 50 m*M* KCl and concentrated via centrifugal filtration to 0.5–1.2 m*M* in 90% H_2O:10% D_2O.

Main chain amide NMR spectral assignments

^{15}N-HSQC spectra were recorded at 35°C at pH 3.8 on a Varian Unity 500 MHz spectrometer, processed using NMRpipe[49] and analyzed using SPARKY 3.0.[50] Chemical shifts were referenced to an external sample of 2,2-dimethyl-2-silapentane-5-sulfonic acid (DSS). The amide ^{15}N-$^{1}H^{N}$ resonances of ^{15}N-labeled WT HEWL were assigned based on published data.[51] To ensure that all cross-peaks in the ^{15}N-$^{1}H^{N}$ HSQC were tracked correctly with increasing pH, the ^{15}N and $^{1}H^{N}$ chemical shifts were verified with a ^{15}N-NOESY-HSQC at pH 7.3. The ^{15}N-$^{1}H^{N}$ resonances of the 9 ^{15}N-labeled HEWL single mutants, E7Q, H15A, D18N, E35A, D48N, D52N, D66N, D101N, and D119N, were assigned by comparison to the WT. In the case of D52N, which showed more extensive spectral changes, the amide resonances were assigned using additional ^{15}N-NOESY-HSQC and ^{15}N-TOCSY-HSQC[52] NMR experiments.

Side chain amide NMR spectral assignment

Spectra were recorded at 35°C on a cryoprobe-equipped Varian Inova 600 MHz spectrometer. Signals from the side chain ^{13}C and ^{1}H nuclei of the Asp and Glu residues in WT HEWL were assigned via a suite of standard 3D $^{1}H/^{13}C/^{15}N$ correlation experiments, with consideration of published chemical shift data.[51,53,54]

This included the stereospecific assignments of the $H^{\beta 1/\beta 2}$ and $H^{\gamma 1/\gamma 2}$ by referencing to the published data above. The signals of the His15 $^{13}C^{\varepsilon 1/\delta 2}$ nuclei in constant time (CT) ^{13}C-HSQC spectra were assigned based on comparisons to the published chemical shifts.[53]

pH titrations of HEWL by NMR spectroscopy

The pH values of the samples were adjusted in steps of approximately 0.2–0.3 increments using dilute HCl or NaOH. Sample pH values were recorded immediately before and after recording NMR spectra using a pH meter (MeterLab PHM220, Sigma), calibrated at room temperature (~21°C) with standard buffer solutions. Typically the initial sample was acquired at pH 3.8, and then pH was lowered in steps of 0.2–0.3 units to pH 2. The sample pH was raised back to pH 3.8 and recorded to check the reversibility of the sample as a function of pH. The pH of the sample was finally increased to pH 8–9 in 0.2–0.3 increments. No corrections were made for the small isotope effect from 10% D_2O, or for recording the NMR data at 35°C. The estimated ionic strength was ~0.05*M*. Insoluble fractions of the protein were pelleted by centrifugation and removed from the sample before recording spectra.

The pH-dependent carbonyl $^{13}C^{\gamma/\delta}$ signals of the Asp and Glu carboxyl groups, and of the C-terminal Leu in $^{13}C/^{15}N$-labeled WT HEWL were monitored using 2D $H_2(C)CO$[55,56] experiments to provide $^1H^{\beta/\gamma}$-$^{13}C^{\gamma/\delta}$ correlations. The pH-dependent $^{13}C^{\delta}$-$^1H^{\delta}$, $^{13}C^{\varepsilon}$-$^1H^{\varepsilon}$, and $^{13}C^{\zeta}$-H^{ζ} signals of aromatic sidechains were monitored using CT ^{13}C-HSQC experiments. The pH-dependent $^{15}N^H$-H^N signals from the WT and mutant ^{15}N-labeled HEWL samples were monitored using ^{15}N-HSQC experiments.

The raw data from the pH-dependent titrations of the $^1H^{\alpha/\beta}$ signals of the ionizable residues in WT HEWL were kindly made available by Christina Redfield.[40]

Titration curve fitting

The pH-dependent chemical shifts of ^{13}C, ^{15}N and ^{1}H nuclei (including those from Bartik and co-authors) were fit to obtain the apparent pK_a values of the ionizable residues. As described in the introduction, the monitored titration curves were fit to permutations of the HH equation (Eqs. 1 and 3) using an in-house program Ekin.[18] All titration curves were uploaded to a database (Protein Engineering Analysis Tool DataBase, PEAT_DB[33]). The appropriate model for fitting a specific titration curve was selected manually to give the lowest overall R^2. Although we advocate the use of an automatable F-test for selecting the appropriate model,[18] here we used manual inspection to spot artifacts and manually remove outliers, and to emulate the fitting process used for most pK_a values reported in literature.

Standard deviations of fitted titration curves

We determined the standard deviations of the reported pK_a values by randomly perturbing individual pH data points by ±0.1 units and the chemical shift components by ±0.02 ppm (^{1}H), ±0.05 ppm (^{15}N), and ±0.2 ppm (^{13}C), and refitting the experimental curve. For each curve we performed 50 refits and use the resulting 50 pK_a values to calculate the standard error on each pK_a value. It should be noted that the magnitude of the random perturbation of chemical shift values must be adjusted to model the error of a given NMR spectrum accurately. The values given here may be too high or too low for other types of spectra and depend on a subjective assessment of spectral quality and the ease with which peaks can be tracked.

Identifying titratable groups that are responsible for ghost titrations

To identify the chemical titrations responsible for producing ghost titrations in remote nuclei, we constructed nine site-directed mutants of HEWL (E7Q, H15A, D18N, E35A, D48N, D52N, D66N, D101N, D119N). Titration curves of the backbone amide ^{15}N and $^1H^N$ nuclei were recorded with ^{15}N-HSQC spectra for all of the nine mutant proteins and compared to those of the wild type protein. A titratable group was identified as being responsible for a ghost titration observed in the wild type if the titration in question was absent only in the mutant examined (i.e., the titration must be present in all other mutants), and if the absolute magnitude of the chemical shift change was >0.2 ppm for ^{15}N, and >0.05 ppm for $^1H^N$.

Preparation of PDB files for pK_a calculations

The atomic co-ordinates of WT HEWL were taken from PDB ID 2LZT.[57] The PDB file was regularized using WHAT IF.[58] All crystallographic water molecules were eliminated from the PDB files and all missing protein atoms were rebuilt using WHAT IF.

pK_a calculations

pK_a calculations were performed using the WHAT IF routines previously described,[59] with the exception that a uniform protein dielectric constant of eight was used. The Poisson-Boltzmann equation (PBE) solver DelPhi II[60] was used to obtain the electrostatic energies with the following parameters: number of focusing runs, four; final PBE map resolution, 0.25 Å/grid point; protein dielectric constant, 8; solvent dielectric constant, 80; ionic

strength, 144 m*M*; ionic exclusion radius, 2.0 Å; solvent probe radius, 1.4 Å. Titratable groups included in the pK_a calculations were the N-terminal amine, all Asp, Cys, Glu, His, Lys, Arg, and Tyr residues, and the C-terminal carboxyl. Only the transition from neutral to positively charged was included for the histidine.

RESULTS

The pK_a values of HEWL have been reported in several studies over the last 4 decades (Table I), and these pK_a values generally agree reasonably well. However, the importance of NMR-measured pK_a values for the study of protein electrostatics in general, and for the benchmarking of protein pK_a values, warrants a detailed study on the actual accuracy of these data. Therefore, we re-measured the NMR pH-titration curves of all carboxyl moieties and the single histidine residue of WT HEWL. We analyzed the titration curves recorded from two wt HEWL samples (one ^{15}N-labeled and the other $^{15}N/^{13}C$-labeled) using the NMR experiments described in Materials and Methods. In parallel, we re-analyzed the raw chemical shift data recorded from 2D ^{1}H spectra as obtained from Bartik *et al.*[40] To identify the source of the titrations reported by the backbone amide protons and nitrogens, we also measured the titration curves for these nuclei in ^{15}N labeled samples of nine HEWL mutants (E7Q, H15A, D18N, E35A, D48N, D52N, D66N, D101N, and D119N).

Spectral quality

The 129 amino acid WT HEWL yielded excellent quality and well-dispersed NMR spectra from the HSQC experiments. Supporting Information Figure SI1 shows the ^{1}H-^{15}N HSQC spectrum of WT HEWL at 35°C and pH 3.8, with the backbone amide ^{15}N-$^{1}H^{N}$ and indole $^{15}N^{\varepsilon 1}$-$^{1}H^{\varepsilon 1}$ assignments indicated. The data are comparable to those published by Buck and co-authors,[51] and this enabled us to use the Buck data for peak assignments.

WT HEWL NMR titration curves

Following peak assignment, we tracked the pH-dependence of the NMR chemical shifts of the following nuclei: $^{13}C^{\gamma}$ and $^{1}H^{\beta}$ for Asp, $^{13}C^{\delta}$ and $^{1}H^{\gamma}$ for Glu [Supporting Information Fig. SI2(a)], $^{13}C^{\varepsilon 1}$-$^{1}H^{\varepsilon 1}$ and $^{13}C^{\delta 2}$-$^{1}H^{\delta 2}$ for His [Supporting Information Fig. SI2(b)], and $^{13}C'$-$^{1}H^{\alpha}$ for the C-terminal Leu129. In addition the pH-dependent chemical shifts were tracked for the side-chains of Phe ($^{13}C^{\varepsilon 1/2}$-$^{1}H^{\varepsilon 1/2}$, $^{13}C^{\delta 1/2}$-$^{1}H^{\delta 1/2}$, and $^{13}C^{\zeta}$-$^{1}H^{\zeta}$), Trp ($^{13}C^{\delta 1}$-$^{1}H^{\delta 1}$, $^{13}C^{\varepsilon 3}$-$^{1}H^{\varepsilon 3}$, $^{13}C^{\xi 2/3}$-$^{1}H^{\zeta 2/3}$, and $^{13}C^{\eta 2}$-$^{1}H^{\eta 2}$), and Tyr ($^{13}C^{\varepsilon 1/2}$-$^{1}H^{\varepsilon 1/2}$ and $^{13}C^{\delta 1/2}$-$^{1}H^{\delta 1/2}$), as well as for the Gly ($^{13}C'$-$^{1}H^{\alpha}$) residues. This yielded a total of 168 titration curves for wild type HEWL. The pH-dependent chemical shifts of most backbone ^{15}N and $^{1}H^{N}$ nuclei and side chain amide ^{15}N and ^{1}H nuclei were monitored, yielding a further 326 titration curves. Finally, the 26 ^{1}H chemical shift titration curves made available to us from the study of Bartik *et al.*,[40] increased the overall total to 520 titration curves. Over the pH range of 2 - 9 examined, these curves likely arise from the ionization equilibria of the 7 Asp, 2 Glu, 1 His, and N- and C-termini of the protein (and not from the Lys, Arg, and Tyr residues with expected pK_a values >10).

The observed titration curves

We investigate how many of the groups in the dataset can be represented by one, two, three or four apparent pK_a values by fitting all titration curves to permutations of the HH equation Eq. (1) for uncoupled titrations. The "best" model used to fit each titration curve was selected manually since this is the usual practice in the field, and therefore gives a reliable estimate of the error inherent in this process. Furthermore, a manual inspection of each titration curve allows the researcher to double-check peak assignments and remove outliers that originate from broad/misassigned NMR peaks. Of the 520 WT titration curves in the dataset, 94 were fitted to one pK_a value, 205 were fitted to two pK_a values, 69 were fitted with three pK_a values and a single curve was fit to four pK_a values (the ^{15}N titration curve of Cys76). 151 curves could not be fit satisfactorily with less than 4 pK_a values, indicating that we could not discern any significant titrational events from this data. Table II shows the breakdown of these fitting statistics for each type of chemical shift measured in our dataset.

Table II shows that the complexity of the chemical shift titration curves generally increases with the distance between the titratable site and the monitored nucleus. Of the 168 titration curves measured using ^{1}H-^{13}C correlation experiments with a $^{13}C/^{15}N$-labeled WT HEWL sample, 37 were adequately fit to one pK_a value while 59 reported two or more pK_a values and 72 curves could not be fitted. However, the number of titration curves with more than one pK_a value dropped to just 5 if we only considered titration curves measured at atoms that are part of a titrating side chain (the carboxyl ^{13}C of the Asp and Glu residues and the C-terminal Leu129, as well as the imidazole ^{13}C and ^{1}H of His15). Of the titration curves measured using the double-labeled sample at other atoms in the titratable residue (i.e., atoms further away from the site of titration), 11 report more than one pK_a value, while 43 of the titration curves measured at atoms of nontitratable groups (e.g. $^{1}H^{\alpha}$ on Gly) report more than one pK_a value.

Curves displaying only one dominant titration can mostly be fit unambiguously, whereas curves with two or

Table II
Fitting NMR Measured Titration Curves for WT HEWL to Model Fits

Sample	Experiment	Nucleus	1 pK_a	2 pK_a	3 pK_a	>3 pK_a	No fit	Total
Unlabelled	COSY	$H^{\alpha/\beta}$	13	8	1	0	4	26
^{15}N	^{15}N-HSQC	^{15}N	24	82	29	1	27	163
^{15}N	^{15}N-HSQC	$^{1}H^{N}$	20	65	30	0	48	163
$^{13}C/^{15}N$	$H_2(C)CO$	$^{1}H^{\beta/\gamma}$ (D/E)	5	9	0	0	3	17
$^{13}C/^{15}N$	$H_2(C)CO$	$^{1}H^{\alpha}$ (G/C-term)	2	1	0	0	22	25
$^{13}C/^{15}N$	$H_2(C)CO$	$^{13}C^{\gamma/\delta}$ (D/E)	12	4	1	0	0	17
$^{13}C/^{15}N$	$H_2(C)CO$	$^{13}C'$ (G/C-term)	5	4	1	0	15	25
$^{13}C/^{15}N$	CT ^{13}C-HSQC	^{13}C ring (F/Y/W)	9	19	0	0	12	40
$^{13}C/^{15}N$	CT ^{13}C-HSQC	^{13}C ring (H)	1	1	0	0	0	2
$^{13}C/^{15}N$	CT ^{13}C-HSQC	^{1}H ring (F/Y/W)	2	11	7	0	20	40
$^{13}C/^{15}N$	CT ^{13}C-HSQC	^{1}H ring (H)	1	1	0	0	0	2
Total #			94	205	69	1	151	520

The number of titration curves for each data set where a reliable fit can be obtained with a specific model and number of pK_a values.

more titrations often can be fit equally well with a number of parameter combinations, especially in cases where the pK_a values are close and the chemical shift changes for each titration are similar. This fact makes pK_a values from single-transition curves more reliable, especially if both the starting and ending plateaus of the titration are well determined. Viewing the data in Table II in this light, it is clear that titration curves measured close to the ionizable moiety generally contain fewer titrations and therefore will produce more reliable pK_a values.

Magnitudes of the chemical shift changes

The magnitude of the chemical shift change ($\Delta\delta$) is a key factor when extracting a pK_a value from a titration curve. Curves that display larger overall shift changes generally yield better fits since the errors associated with peak tracking become smaller compared to the overall change in chemical shift. The magnitude of the chemical shift change is important because the position of an NMR peak can be measured with limited precision. In addition, curves where a single titration dominates the chemical shift change generally also give more reliable fits.

We compared the chemical shift differences recorded for all titrations in the WT dataset, and found that the ^{13}C nuclei generally exhibit the largest chemical shift change and therefore give more reliable pK_a value measurements. The ^{13}C nuclei closest to a titratable group display chemical shift changes from 1.6 to 4.3 ppm [avg. 2.7 $\pm$ 1.0 ppm] (for Asp $^{13}C^{\gamma}$), 2.5 to 2.9 ppm [avg. 2.6 $\pm$ 0.17 ppm] (for Glu $^{13}C^{\delta}$) and 1.1 to 1.6 ppm (for His 15 $^{13}C^{\varepsilon 1/\delta 2}$). These values generally agree with those found in TitrationDB[18] and with those reported for model compounds.[61,62] Note that the number of titratable groups in HEWL is too low to produce averages and standard deviations with a general validity, and in the following we only report ranges. Chemical shifts for side chain protons closest to the titratable groups produce pH-dependent chemical shift changes of much smaller magnitude (0.05–0.40 ppm for Asp, 0.13–0.37 ppm for Glu) and hence often yield much noisier titration curves than those derived from ^{13}C signals.

The pH-dependent chemical shifts of the amide backbone ^{15}N and $^{1}H^{N}$ nuclei are highly dependent on the distance and orientation to the titratable group responsible for inducing the chemical shift change. In the current dataset we observe ^{15}N chemical shift changes ranging from 0.23–1.9 ppm (Asp), 1.2–1.8 ppm (Glu), and 2.5 ppm (His15), and backbone amide $^{1}H^{N}$ chemical shift changes take values from 0.02–0.13 ppm (Asp), 0.05–0.22 ppm (Glu), and 0.09 ppm (His15). Note that since HEWL contains only one histidine residue, the values are simply the chemical shift difference from the fit of the His15 titration curve. Similarly values for Glu are derived from Glu7 and Glu35.

pK_a values from optimal sites

Because an ionization event typically influences the chemical shift of more than one nucleus, it is possible to measure a given pK_a value via several reporter signals. The titration curves reporting the ionization of a specific group should all fit to the same pK_a value regardless of which nucleus is tracked. However, it is often found that titration curves, and therefore the extracted pK_a values, differ depending on which chemical shift data set is analyzed. It is therefore desirable to use a set of nuclei which provide the most "trustworthy" titration curves and hence the most accurate pK_a values.

In the following we refer to this set of nuclei as the set of "optimal sites" for obtaining pK_a values. When choosing the optimal site for monitoring the titration of a specific titratable group, the magnitude of the chemical shift change and the simplicity of the observed NMR pH-titration curves are the parameters that influence the reliability of the extracted pK_a values. Therefore, the choice typically falls on the nucleus closest to the titration site as measured by the number of bonds that separate the nucleus from the titratable group. Thus the ^{13}C carboxyl

and histidine ^{1}H, ^{13}C, and ^{15}N imidazole nuclei of a titratable group should better reflect the titrations of these ionizable moieties than the other side-chain and main-chain nuclei.

Table III lists the set of apparent pK_a values extracted from the optimal ^{13}C-based titration curves measured in this study. The table furthermore shows the apparent pK_a values extracted from chemical shift titration curves of backbone amide nitrogen and protons, and side chain protons. While there is good agreement between many of the pK_a values, it is also clear that significant differences exist. An example of this is the difference of 1.0 unit in the case of Asp87 (^{13}C vs. ^{15}N), while the discrepancy for the C-terminus is around 0.8 units (^{13}C vs. ^{15}N). The RMSD values to the optimal (^{13}C) pK_a values are given in the final row of the table, and RMSD values as high as 1.3 (^{13}C vs. ^{15}N) is observed with the correlation between side chain proton pK_a values being closer to the ^{13}C values (RMSD = 0.4). The RMSD between pK_a values calculated with two pK_a calculation packages (PropKa[13] and the pKD server/WHAT IF packages[63,64]) is observed to be 0.8 and 0.9 respectively, thus demonstrating that the accuracy of predicted pK_a values approaches the variation in pK_a values between different types of NMR measurements on the same protein. This observation should in no way be taken as a license to construct pK_a calculation methods with lower accuracy since most ^{13}C pK_a values are very accurate. Instead this should remind theoreticians that differences in the performances of pK_a calculation packages translate into meaningful conclusions on protein electrostatics only if the differences in performance are larger than the experimental uncertainty of the dataset used.

The full set of pK_a values from the four NMR experiments analyzed in this work are given in Supporting Information Table SI1 (side chains) and Table SI2 (main chain). In all cases we report the number of bonds from the titration site to the monitored nuclei, the fit pK_a value (where more than one pK_a value is reported, only the major pK_a value is listed in the table), the standard error, and the model to which the titration curve is fit, (i.e., 1, 2 or 3 pK_a values). The sheer number of extracta-

Table III
Measured pK_a Values: ^{13}C, ^{15}N, and ^{1}H

Group	^{13}C	^{15}N	$^{1}H^{N}$	$^{1}H^{\alpha}$	^{1}H side chain	pKD server	PropK$_a$
E7	2.6 ± 0.14 C^{δ}-$H^{\gamma1}$ 2.7 ± 0.12 C^{δ}-$H^{\gamma2}$	3.0 ± 0.05	3.9 ± 0.02	2.6 ± 0.01[a]	2.6 ± 0.04 $H^{\gamma1}$ 2.5 ± 0.03 $H^{\gamma2}$	3.0	3.74
H15	5.5 ± 0.04 $C^{\varepsilon1}$-$H^{\varepsilon1}$ 4.8 ± 0.16 $C^{\delta2}$-$H^{\delta1}$	5.7 ± 0.17	5.6 ± 0.04	—	2.2 ± 0.01 $H^{\beta1}$ [a] 5.3 ± 0.06 $H^{\beta2}$ [a] 6.9 ± 0.03 $H^{\delta2}$ 5.5 ± 0.01 $H^{\varepsilon1}$	4.3	7.25
D18	2.9 ± 0.13 C^{γ}-$H^{\beta1/2}$	3.1 ± 0.05	2.4 ± 0.02	—	2.6 ± 0.05 $H^{\beta1}$ 2.5 ± 0.06 $H^{\beta2}$ 2.7 ± 0.05 $H^{\beta1}$ [a] 2.2 ± 0.03 $H^{\beta2}$ [a]	2.8	2.94
E35	6.0 ± 0.13 C^{δ}-$H^{\gamma1}$ 4.7 ± 0.15 C^{δ}-$H^{\gamma2}$	6.8 ± 0.03	6.4 ± 0.04	—	4.7 ± 0.01 $H^{\beta1}$ [a] 6.1 ± 0.03 $H^{\gamma1}$	5.5	5
D48	1.6 ± 0.06 C^{γ}-$H^{\beta1/2}$ 1.6 ± 0.07 C^{γ}-$H^{\beta2}$	3.8 ± 0.12	3.0 ± 0.10	—	1.4 ± 0.01 $H^{\beta1}$ [a] 1.2 ± 0.01 $H^{\beta2}$ [a] 2.1 ± 0.03 $H^{\beta1}$ 2.7 ± 0.02 $H^{\beta2}$	2.8	1.41
D52	3.6 ± 0.04 C^{γ}-$H^{\beta1}$ 3.7 ± 0.03 C^{γ}-$H^{\beta2}$	4.0 ± 0.03	3.6 ± 0.02	3.4 ± 0.01[a]	3.7 ± 0.02 $H^{\beta1}$ [a] 3.6 ± 0.06 $H^{\beta2}$ [a] 3.7 ± 0.03 $H^{\beta2}$	1.5	3.19
D66	1.1 ± 0.14 C^{γ}-$H^{\beta1/2}$	3.4 ± 0.22	3.7 ± 0.06	1.4 ± 0.00[a]	1.1 ± 0.02 $H^{\beta1}$ [a] 2.2 ± 0.01 $H^{\beta1/2}$	1.8	1.3
D87	2.1 ± 0.07 C^{γ}-$H^{\beta1}$ 2.1 ± 0.05 C^{γ}-$H^{\beta2}$	3.1 ± 0.15	3.2 ± 0.02	2.1 ± 0.03[a]	2.1 ± 0.02 $H^{\beta2}$ [a] 2.3 ± 0.03 $H^{\beta2}$ 1.4 ± 0.03 $H^{\beta1}$	1.4	2.08
D101	4.5 ± 0.02 C^{γ}-$H^{\beta1/2}$	4.5 ± 0.03	3.8 ± 0.02	3.4 ± 0.01[a]	4.5 ± 0.02 $H^{\beta1/2}$	4.4	4.01
D119	3.0 ± 0.05 C^{γ}-$H^{\beta1}$ 3.5 ± 0.07 C^{γ}-$H^{\beta2}$	3.4 ± 0.05	3.9 ± 0.01	3.2 ± 0.03[a]	3.2 ± 0.02 $H^{\beta1}$ [a] 3.7 ± 0.01 $H^{\beta1}$ 3.7 ± 0.01 $H^{\beta2}$	3.2	3.48
Cterm	3.9 ± 0.19 C′- H^{α}	3.1 ± 0.04	3.0 ± 0.05	2.8 ± 0.02[a]	2.7 ± 0.02 $H^{\beta1}$	2.4	2.64
RMSD	—	1.3	1.2	0.6[b]	0.4	0.9	0.8

Group: titratable residue. ^{13}C pK_a value (average): pK_a values measured using the indicated correlations in $H_2(C)CO$ or ^{13}C-HSQC spectra. ^{15}N: pK_a values measured at backbone amide nitrogens. $^{1}H^{N}$: pK_a value measured at the backbone amide proton. $^{1}H^{\alpha}$ pK_a values measured at the Hα proton. ^{1}H side chain: pK_a values measured at side chain protons.
RMSD: The root mean square deviation between the pK_a values in each column and the pK_a values in the ^{13}C column. We use the average pK_a value for the RMSD calculation if more than one pK_a value is measured for a titratable group at a specific site. It is seen that the difference between the sets of experimental measurements is similar in size to the differences in the calculated results and the "best" set of pK_a values.
"—," No titration curve available.
[a] A measured pK_a value from fitting the raw chemical shift. Data supplied by Bartik and co-authors (Bartik et al., 1994).[40]
[b] $^{1}H^{\alpha}$ RMSD value calculated using the 7 available pK_a values.

ble pK_a values even for a small protein such as HEWL clearly shows that the assignment of apparent pK_a values to specific ionizable groups is not a trivial task.

Variation in measured pK_a values

Table III, and Supporting Information Tables SI1 and SI2, summarize the differences in the pK_a values that can be obtained from fitting the titration curve of various nuclei associated with ionizable side chains. From these data, it is evident that titration curves that typically would be assumed to report the same titrational event can yield very different pK_a values. The extent of the variation in the pK_a values is illustrated in Figure 2, where the pK_a value associated with the titration displaying the largest chemical shift change is plotted for each atom within the titratable groups in HEWL. The spread of fit pK_a values for each individual titratable group is very large, with only a few residues displaying a variation of less than 1 unit. The variation in the measured pK_a values is furthermore qualitatively correlated with the number of titratable groups close to the group of interest. Relatively isolated groups tend to display less variation in the measured pK_a values, whereas groups in highly charged environments tend to display a larger variation. This observation suggests that the variation in the observed pK_a values is due to ghost titrations being overlaid and thus obscuring the "self" titration for a given residue.

To gain an insight into the variation of the extracted pK_a values it is instructive to examine a number of potential reasons for the variation. In the following we comment on the role of cross peak pK_a differences, structural variation, long-range electrostatic effects and the fitting procedure for titration curves displaying multiple transitions.

Cross peak differences in pK_a values

The titration curves obtained from two cross peaks for the same nucleus in a given spectrum (i.e., the $^{13}C^{\gamma}$ chemical shift from the pair of $^{13}C^{\gamma}$-$^{1}H^{\beta 1}$ and $^{13}C^{\gamma}$-$^{1}H^{\beta 2}$ peaks for an Asp residue in a $H_2(C)CO$ spectrum) should display the same titration curve and therefore must fit to the same pK_a value. Reassuringly, in the case of HEWL most differences in pK_a values measured from two cross peaks for the same nucleus are very low ($\leq$0.1 pK_a unit). However, we observe a 0.5 unit difference in

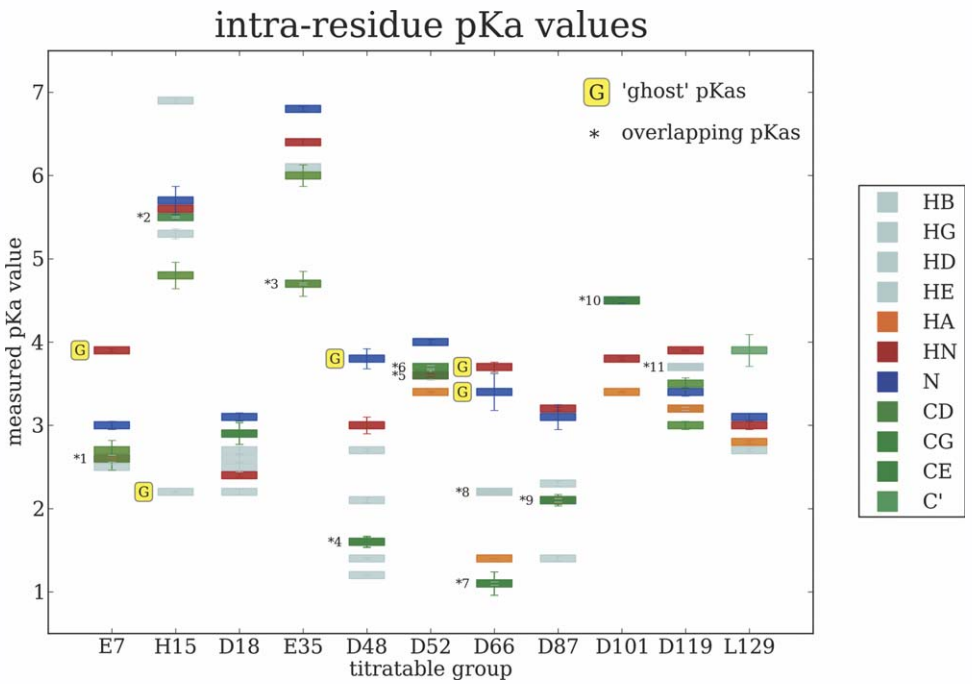

Figure 2

The pK_a values associated with the largest chemical shift change in the NMR pH-titration curves of nuclei within the Asp, Glu, His and C-term residues of wild type HEWL. The spread in pK_a values is larger for groups that are situated in highly charged regions of the protein, whereas isolated titratable groups display a tighter distribution of pK_a values. (G): represents a ghost titration, *x: represents overlapping pK_a values measured using the chemical shifts for the following atoms/cross peaks: (1) C^{δ}-$H^{\gamma 1}$ crosspeak, the $H^{\gamma 1}$ and the H^{α} atoms in E7; (2) $C^{\varepsilon 1}$ and $H^{\varepsilon 1}$ atoms in H15; (3) C^{δ}-$H^{\gamma 2}$ crosspeak and the $H^{\beta 1}$ atom in E35; (4) C^{γ}-$H^{\beta 1/2}$ crosspeaks for D48; (5) C^{γ}-$H^{\beta 1}$ crosspeak and the $H^{\beta 2}$ and H^{N} atoms in D52; (6) C^{γ}-$H^{\beta 2}$ crosspeak and the $H^{\beta 1}$ atom in D52; (7) C^{γ}-$H^{\beta 1/2}$ crosspeaks and the $H^{\beta 1}$ atom in D66; (8) $H^{\beta 1/2}$ atoms in D66; (9) C^{γ}-$H^{\beta 1/2}$ crosspeaks and the H^{α} and $H^{\beta 2}$ atoms in D87; (10) C^{γ}-$H^{\beta 1/2}$ crosspeaks and the $H^{\beta 1/2}$ and N^{H} atoms in D101; (11) $H^{\beta 1/2}$ atoms in D119.

the pK_a values for Asp119 extracted from its $^{13}C^{\gamma}$-$^{1}H^{\beta1}$ and $^{13}C^{\gamma}$-$^{1}H^{\beta2}$ titration curves, thus demonstrating that in specific cases erroneous peak assignment, peak overlap and/or broad peaks can produce differences in titration curves. We expect pK_a value differences of the magnitude indicated for Asp119 to be rare in published values, but nevertheless note that such cross-validation of pK_a values is important.

Structural variation

Another potential reason for the discrepancy between pK_a values is that nuclei are not equally sensitive to structural alterations. The titration of a nearby ionizable group can induce subtle changes in the chemical environment, for example, an H^{β} in a different residue. These pH-dependent changes are not necessarily felt by the H^{α} in the titrating residue, and can thus give rise to different titration curves and pK_a values for the two protons. Such phenomena can also be observed when rotamer populations change as a result of titrational events, or when larger-scale pH-dependent conformational changes occur.[25] Indeed each nucleus in a protein has the potential to be unique (freely rotatable protons are mostly not) and thus produce a unique titration curve reflecting its sensitivity and the pH-dependent changes in its environment.

Long-range electrostatic effects

Atoms connected by a highly polarizable covalent bond are extremely sensitive to changes in the electrostatic field, and this often causes titration curves measured at the backbone amide atoms (^{15}N and $^{1}H^{N}$) to be dependent upon several titrational events. Titration curves that report multiple ionization equilibria are typically more difficult to fit, and they can sometimes be described equally well by several different models. In addition to the problem associated with fitting the titration curves, it is also difficult to know exactly which titration is being tracked since even distant titrational events can have a large influence on the chemical shift. We therefore expect pK_a values from main chain amide atoms to be less reliable than pK_a values obtained from titration curves obtained from the chemical shift perturbation of other atoms. This is supported by the data in Figure 2 since pK_a values measured at main chain amide atoms often present outliers or ghost titrations in the plot.

Reconciliation of pK_a values and ^{15}N titration curves

It is clear that peak tracking and erroneous peak assignment can have an impact on pK_a values. However, other sources of variation such as sample conditions, calibration of pH-meters, the differential sensitivity of nuclei to electrostatic effects and environmental changes, and the difficulty of fitting curves displaying multiple titrations are also likely to play major roles. It is also possible that the variation in apparent pK_a values can be explained by the difficulty of accurately fitting multiphasic titration curves. If this is the case, then it should be possible to use the pK_a values derived from the carboxyl ^{13}C chemical shifts to guide the fits of the more complicated titration curves. If we successfully can fit all titration curves using a single set of pK_a values for the ionizable groups in a protein, it means that our fitting procedures for individual residues are responsible for the observed variation in pK_a values.

We fit the ^{15}N titration curves of all titratable Asp, Glu and His residues using the pK_a values extracted from the carboxyl/imidazole ^{13}C chemical shifts of their side chains. The results of this exercise are shown in Figure 3. In some cases (Glu7, His15, Asp18, Asp52, Asp66, Asp101, and Asp119), the use of pK_a values obtained from side chain carboxyls fits the ^{15}N titration curves. However, Asp48 does not report its own titration and therefore cannot be fitted. For residues Glu35 and Asp87, the ^{15}N titration curves simply cannot be fit satisfactorily to pK_a values obtained from carboxyl $^{13}C^{\gamma/\delta}$ shifts of these residues. In the case of E35, the pK_a value of 6.1 is too low, and similarly for Asp87 the pK_a value of 2.2 is too low to fit to the ^{15}N titration curve.

It should be mentioned that although we can achieve good correlations between the ^{13}C pK_a values and the ^{15}N titration curves, we often had to use an equation with 1-2 extra pK_a values. This procedure sometimes immediately yielded pK_a values that were close to those measured for other titratable groups, but typically the "additional" pK_a values could be altered quite significantly. Furthermore, often the best fits were obtained only when using carefully selected starting values thus illustrating the considerable uncertainty and multiple local minima associated with the fitting procedure. For example, in the case of Asp52 we could achieve a satisfactorily agreement only when using three pK_a values, one of which was 3.6 (the ^{13}C carboxyl pK_a value of Asp52). However, the additional two pK_a values in the model could vary over a wide range and produce fits of almost identical quality. Supporting Information Table S3 details the pK_a values used when fitting the curves in Figure 3, but it should be pointed out that many of these pK_a values could vary considerably and therefore should be interpreted carefully.

Differences in pK_a values

As evident from the above results, there can be a significant spread in the pK_a values attributed to the same ionizable group when the titration curves are measured using the chemical shifts of different nuclei. However, the titration curves can of course also be different due to

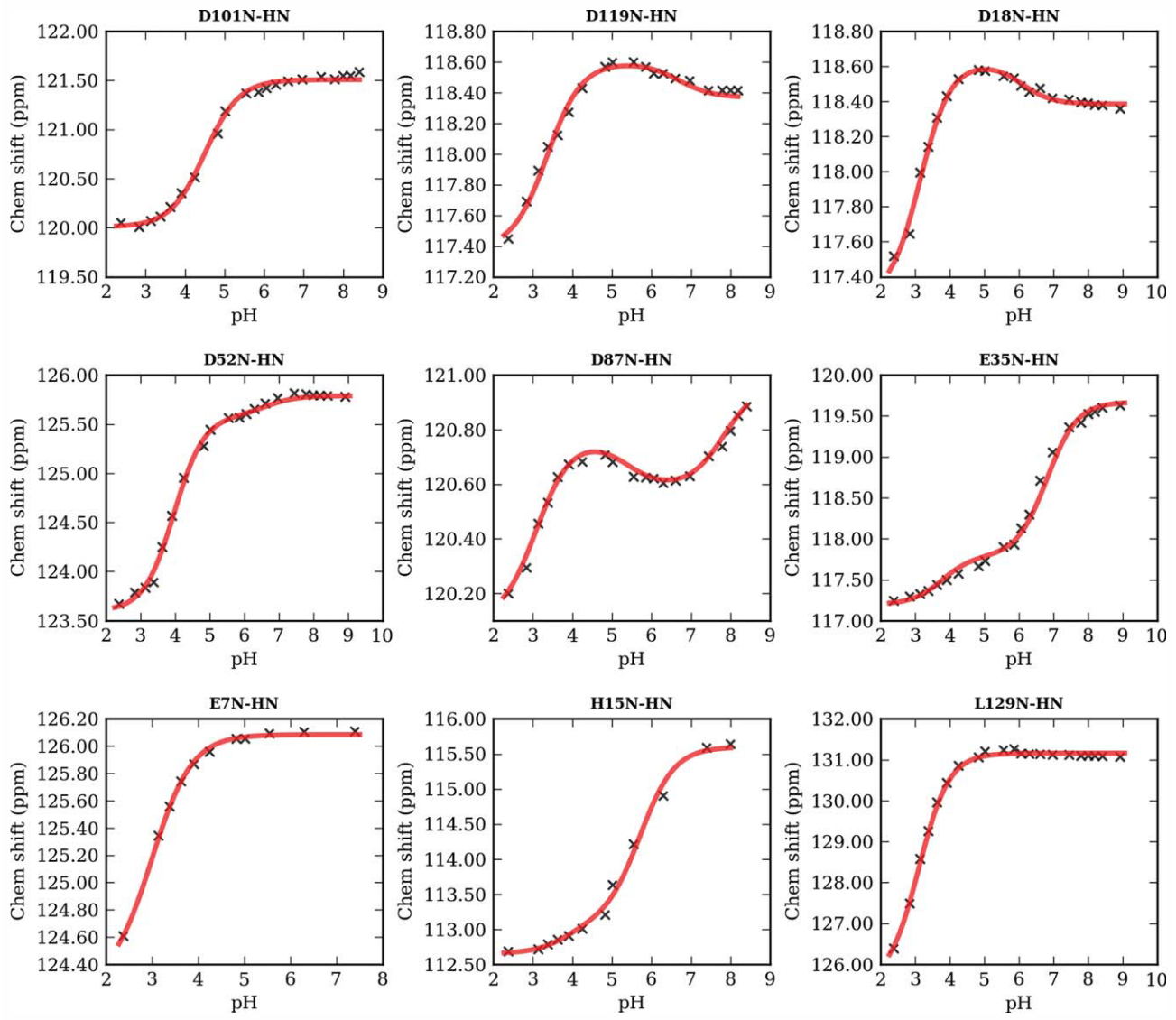

Figure 3

The amide ^{15}N titration curves of His15 and all Asp/Glu residues except Asp48 fit using the major pK_a value determined from the ^{13}C titration curve of the same residue. The titration curves were fit to models describing one (Asp101, C-term), two (Glu7, Glu35, Asp119), or three (His15, Asp18, Asp52, Asp66, Asp87) sequential ionizations, with only one pK$_a$ kept fixed according to the ^{13}C titration data. The ^{15}N titration curve of Asp48 does not report its own ionization and was therefore not included in the plot. The titration curves of Glu35 and Asp87 were not possible to reconcile with the ^{13}C pK$_a$ values of these residues. For Asp87, with a carboxyl pK$_a$ value of 2.2, the titration curve can be fit well with pK$_a$ values of 2.8 (presumably Asp87), 5.5 (His15), and 7.5 (unknown), The titration curve for Glu35, with a carboxyl pK$_a$ value of 6.1, can be fit to pK$_a$ values of 3.8 (presumably Asp52) and 6.6 (presumably Glu35). Figure produced using EKIN.[33] [Color figure can be viewed in the online issue, which is available at wileyonlinelibrary.com.]

other factors such as the sample conditions (ionic strength, temperature, buffer), the range and distribution of the pH values examined, and the fitting procedures employed.

The ^{1}H titration curves of Asp101 (with a pK$_a$ of 4.5 ± 0.02 from its $^{13}C^{\gamma}$; Figure 4) illustrate why it is important to record the chemical shift at many pH values over a wide range. The $H^{\beta 1/2}$ (this study) displays two pK$_a$ values (4.5 and 7.5), the $^1H^{\alpha}$ (Bartik *et al.*) also displays two pK$_a$ values (1.4 and 3.4), while the $^1H^N$ (this study) can be fitted well with three pK$_a$ values (3.8, 5.4 and 6.0). In addition to differences that are caused by nuclei monitoring different ionizations, "extra" titrations can be missed and plateaus can be poorly defined if the chemical shift is not measured over the entire pH range. Thus, while Bartik *et al.* observe the titration with a pK$_a$ value of 1.4, they do not observe the high-pK$_a$ titrations associated with the true pK$_a$ of Asp101, and lack the proper definition of a plateau at high pH. This possibly leads to a lower pK$_a$ value for the second titration, and might

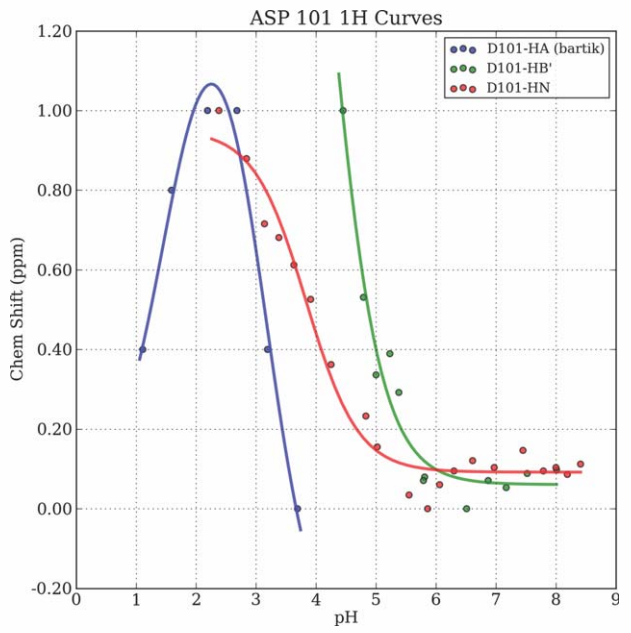

Figure 4

The titration curves observed by monitoring the chemical shift perturbations of the ^{1}H nuclei in Asp101. The H^{N} (red) and $H^{\beta'}$ (green) titration curves were measured in this study, while the H^{α} (blue) curve was obtained by Bartik *et al.* Figure produced using EKIN.[33]

increase the error on the fitted pK_a value. We do not observe the titration with a low pK_a value and no experiments were able to define a plateau at low pH values.

The spacing of the chosen pH values is also important for the correct interpretation of the observed titration curves. Too few pH points can produce curves that appear mono-phasic (HH-shaped), while measurements performed at more pH values clearly shows a bi-phasic behavior. We advocate a separation in pH values of 0.2 units, and the chemical shift should be measured at all pH values where the protein is stable and folded (see Farrell *et al.*[18] for more information).

The error on experimentally measured pK_a values

While we have made significant efforts to reconcile the pK_a values from the different experiments in the above analysis, it is clear that there are still many discrepancies in assigning and fitting titrations of different reporter nuclei to a common acid dissociation equilibrium. These differences are larger than the errors normally reported for experimentally measured pK_a values, which reflect the precision of the data analysis alone.

In our attempts to reconcile the pK_a values we have applied the reliability criteria listed in the introduction: the closer the nucleus is to the site of titration the more reliable the pK_a value, and the simpler a titration curve, the more accurate the pK_a values. However, the discrepancies observed for the ^{13}C pK_a value of His 15 (5.5 and 4.8, measured at the $C^{\varepsilon 1}$ and the $C^{\delta 2}$, respectively) show that significant differences in pK_a values can be observed within the same experiment. It should be mentioned that the discrepancy of the pK_a values extracted from the ^{13}C titration curves from His 15 to a large extent originates from poor data above pH 5.2 for $C^{\delta 2}$. By excluding a data point and carefully selecting starting values for the nonlinear fit, we can achieve a good description of the titration curve for $C^{\delta 2}$ with pK_a values of 2.6 and 5.4 (see Supporting Information section on His15 and Figure SI4). However, this slight data manipulation combined with the arguments above, shows that the reliability of assigning experimentally measured pK_a values to specific ionizable groups is far more difficult than might be naively expected.

Table IV provides an overview of the ranges of the pK_a values measured for each titratable group along with an indication of which pK_a value we find to be the best consensus pK_a value for that residue. Overall there is a good agreement between the pK_a values obtained by the different measurement with ΔpK_a values of <0.5–1.0 units. The single exception is in the case of the C-terminal residue, where there is a large discrepancy between the measured pK_a values. Significantly we are not able to resolve the ambiguity of the pK_a values for the C-terminus since the most likely explanation involves the assumption that the chemical shift of the C-terminal carbonyl carbon is not dominated by the ionization of the C-terminal (see Supporting Information Figure SI5 and Discussion).

pK_a values of inter-residue titrations (ghost titrations)

In the final part of this work, we investigated agreement between pK_a values in ghost titrations and those reported by the ^{13}C titration curves. We analyzed the ti-

Table IV
Variation in Measured pK_a Values

Titratable group	pK_a values measured (outliers)	Consensus pK_a value
Glu 7	2.5–2.7 (3.9, 3.9)	2.6 ± 0.2
His 15	5.3–5.7 (4.8, 6.9)	5.5 ± 0.2
Asp 18	2.2–2.9	2.8 ± 0.3
Glu 35	6.1–6.8	6.1 ± 0.4
Asp 48	1.2–1.6 (2.1, 2.7)	1.4 ± 0.2
Asp 52	3.4–4.0	3.6 ± 0.3
Asp 66	1.1–1.4 (2.2)	1.2 ± 0.2
Asp 87	2.1–2.3 (1.4, 3.1, 3.2)	2.2± 0.1
Asp 101	4.5 (3.4, 3.8)	4.5 ± 0.1
Asp 119	3.2–3.9	3.5 ± 0.3
C-terminus	2.4–2.8 (3.9)	2.7 ± 0.2/3.9 ± 0.1

Variation in HEWL pK_a values. Values are given without errors and outliers are given in parentheses. The consensus pK_a value represents our best estimate of the true pK_a value of the residue, with an error that is judged reflecting the variation in the measurements. The C-terminal represents the single major discrepancy ($\Delta pK_a > 1.0$ unit), although the pK_a values of several groups display quite a wide range.

Table V
pK_a Values from Backbone $^1H^N$ and ^{15}N Titrations Curves

Group	$^1H^N$ Own apparent pK_a	Number of mapped proton pK_a values	Average proton pK_a value/std deviation	^{15}N Own apparent pK_a	Number of mapped nitrogen pK_a values	Average nitrogen pK_a value/std deviation
E7	—[a]	5	2.79 ± 0.38	3.0	4	3.04 ± 0.2
H15	5.6	5	5.71 ± 0.24	5.7	6	5.49 ± 0.29
D18	2.4	8	3.21 ± 0.47	3.1	5	3.20 ± 0.06
E35	6.4	18	6.65 ± 0.44	6.8	30	6.62 ± 0.58
D48	—[a]	—	—	—[b]	—	—
D52	3.6	12	3.70 ± 0.39	4.0	13	3.68 ± 0.37
D66	—[a]	1	2.26	—[b]	3	2.36 ± 0.37
D87	3.2	4	2.70 ± 0.68	3.1	2	3.31 ± 0.42
D101	3.8	5	4.22 ± 0.57	4.5	8	4.26 ± 0.24
D119	3.9	1	3.21	3.4	—	—
L129	3.0	3	3.28 ± 0.18	3.1	3	3.55 ± 0.05

Group: The titratable group in WT HEWL (pH 2–9), Own apparent pK_a value: the apparent intra-reside pK_a value reported from the main chain amide of that titration group (i.e., the reported self titration), Number of mapped pK_a values: the number of groups which sensed the inter-reside titration of that titratable group assigned based on the mentioned HEWL mutants and where the chemical shift change of the titration was required to be 0.2 and 0.05, for N and H, respectively, Average pK_a value: the average pK_a value reported by all residues for the titratable group, Std. dev: the standard deviation on the reported pK_a values.
[a]The $^1H^N$ titration of Glu7, Asp48, and Asp66 did not report a self-titration and therefore has no $^1H^N$ reported pK_a value.
[b]The ^{15}N titration of Asp48 and Asp66 did not report a self-titration and therefore has no ^{15}N reported pK_a value.

tration curves for all backbone and side chain amide atoms in wild type HEWL and nine mutants (E7Q, D18N, H15A, E35A, D48N, D52N, D66N, D101N, and D119N). A comparison of these datasets allowed us to identify the titratable groups responsible for most of the inter-residue pH-dependent chemical shift changes observed for the wild type protein. An example was previously shown (see Figure 1) where the ^{15}N titration curve of Asp48 in WT HEWL is compared to the same titration curve in the D52N and E35A mutants. By observing the disappearance of both the low and high titration in the two mutants, we can attribute the titration curve of Asp48 to Asp52 and Glu35 respectively, although it is clear that the residue is influenced by ionization events other than those of Asp52 and Glu35. It is however, in principle, possible to measure the pK_a values of Asp52 and Glu35 by fitting the titration curve of Asp48. Since the titration of a titratable group can be observed at many nuclei, sometimes across the protein, we can therefore calculate an average pK_a value for the titratable groups from these ghost titrations.

We fit all backbone amide nitrogen and proton titration curves to determine pK_a values of their parent residue using the mutant spectra as guidelines. Table V shows the number of such fit ^{15}N and $^1H^N$ titration curves along with the average and standard deviations for each pK_a value. The number of ghost pK_a values observed for a single residue varies from 0 up to 30 titrations being observed in wild type HEWL for a given titration event. Glu35 is responsible for the largest number of inter-residue (ghost titrations), with its ionization reflected by the pH-dependent shifts of 30 reporter ^{15}N nuclei and 18 reporter $^1H^N$ nuclei. Generally the pK_a values extracted from these ghost titrations cluster quite tightly around the pK_a value of the parent titratable group, as determined from measurements on the nuclei in the parent titratable group side chain. The largest variation in the inter-residue pK_a values of the $^1H^N$ and ^{15}N nuclei is noted for Asp87 and Glu35, respectively.

CONCLUSIONS

No systematic studies have been performed to date on the accuracy and agreement of pK_a values obtained by tracking the pH-dependence of the chemical shift for several different types of nuclei. To address these issues, we have compared the NMR-measured pK_a values for HEWL to obtain a realistic estimate of their accuracy. We find large deviations between the apparent pK_a values potentially assignable to the ionization equilibrium of a given residue, with the largest differences observed between those measured at backbone amide atoms versus the remaining atoms. The high sensitivity of the peptide bond to the protein electric field is a major reason for $^1H^N$ and ^{15}N reporting ghost titrations. Although better, the agreement between pK_a values from pH-dependent ^{13}C, $^1H^\alpha$, and side chain proton shifts (RMSD of 0.4) is also not perfect. For example, the $^{13}C^{\varepsilon 1}$ and $^{13}C^{\delta 2}$ within the same imidazole ring of His15 yield apparent pK_a values of 5.5 ± 0.04 and 4.8 ± 0.16 due to difficulties in fitting the poor data above pH 5.2 for $C^{\delta 2}$ (Table III and Supporting Information Fig. SI4), and we are genuinely not able to determine if the C-terminal has a pK_a value of 2.7 or 3.9. Thus, while ^{13}C pK_a values in general undoubtedly are very reliable for many proteins (Supporting Information Table SI4), individual ^{13}C-measured pK_a values can be inaccurate if the titration curves are poor, incomplete, if the system displays conformational changes (e.g. as in thioredoxin) or if the chemical shift simply reports some other titrational event.

Measuring more reliable pK_a values

A reliable pK_a value measurement should always start with a ^{13}C-measured pK_a value obtained using the best practices.[18] Furthermore, each pK_a value should be associated with its estimated true accuracy based on an assessment of the analyzed titration curves and any complementary data. If one performs measurements at multiple nuclei and takes additional experimental information (mutant spectra, pH-activity profiles, pH-stability profiles etc.) into account, it becomes easier to estimate the true accuracy of each pK_a value. For example, one can be very confident of the pK_a values in the well-studied systems *Bacillus circulans* xylanase,[65] Staphylococcal nuclease (SNase)[37,38] and Protein G,[66] whereas other well-studied systems such as thioredoxin[67,68] still cause controversy thus illustrating that the accuracy of pK_a values is highly system-dependent.

The use of experimental data such as pH-activity profiles, mutant proteins and pH-stability profiles may be used to further confirm pK_a value measurements. However it should be noted that pH-stability profiles alone cannot give site-specific measurements and that the interpretation of the properties of mutant proteins often result in circular arguments. Furthermore the use of pH-activity profiles relies crucially on a correct identification of the catalytically competent protonation state of the enzyme, particularly in the case of reverse protonation enzymes, and a verification that the stability of the enzyme does not affect the measured pH-dependence of catalytic activity.[69]

BENCHMARKING THEORETICAL METHODS

The large errors potentially associated with experimentally measured pK_a values should cause the theoretical pK_a calculation community to re-evaluate the benchmarking procedures used to evaluate the performance of pK_a calculation algorithms. When compiling an experimental dataset for benchmarking purposes, a theoretical researcher must assess the accuracy of the pK_a values in the dataset. Such an assessment can, as a first approximation, be based on the NMR method used for measuring the pK_a values. Thus as a cautious first iteration pK_a values measured at backbone amide atoms should be considered accurate only within ± 1.0 unit, pK_a values from side chain protons accurate to within ± 0.5 pK_a units, whereas ^{13}C-derived pK_a values most likely are accurate to within 0.1–0.2 units. Therefore, as a first step, only ^{13}C - measured pK_a values should be used for benchmarking theoretical methods. However, the average accuracy for each type of measurement hides large site-specific variations in each type of pK_a values as demonstrated earlier, and ideally the individual true accuracy of each pK_a value should be used to define the experimental uncertainty of the dataset used.

In the absence of such detailed information, the accuracy of large collections of pK_a values can be produced using a back-of-the-envelope calculation. Such a calculation for the PPD dataset yields a rough estimate of the minimum average error on the pK_a values in this dataset of 0.5 units ($0.66 \times 0.5 + 0.2 \times 0.2 + 0.14 \times 0.7$), and this value should be kept in mind when comparing the performance of different pK_a calculation algorithms on this dataset. A re-examination of the performance of five pK_a calculation algorithms[70] reveals that several performance differences are borderline when taking the estimated accuracy of the experimental pK_a values into account. This average error only includes errors/uncertainties that are due to the inherent inaccuracy of the NMR methods examined here, and does not include errors such as misassignments, poorly designed experiments, incorrect database deposition and different buffer conditions. The inclusion of such errors is likely to result in a substantially larger average error on the pK_a values in the PPD database[19] and indeed any compilation of pK_a values.

To achieve a higher accuracy in future theoretical pK_a predictions, experimental data must be selected carefully for benchmarking, and individual pK_a values should be assigned confidence values to ensure that pK_a values with large errors do not unduly influence the calibration of a pK_a calculation algorithm (i.e., to ensure that researchers do not optimize their methods against experimental noise). Such a careful selection and assessment of experimental pK_a values (which should only consider ^{13}C-measured pK_a values) is only possible if the primary experimental data is available, and we therefore hope that the results presented here will motivate experimental researchers to deposit their raw NMR titration curves, pH-activity profiles, pH-stability profiles and other relevant experimental data in Titration_DB,[18] PEAT_DB[33] or other databases.[71] A collection of carefully measured, publically available NMR titration curves and pK_a values with associated biophysical data would present an invaluable collection of data for theoretical researchers and provide a solid basis for a better understanding of protein electrostatics, the determinants of the NMR chemical shift, and ultimately contribute to a better understanding of protein structure and function.

REFERENCES

1. Warshel A, Sharma PK, Kato M, Parson WW. Modeling electrostatic effects in proteins. Biochim Biophys Acta 2006;1764:1647–1676.
2. Jiang L, Althoff EA, Clemente FR, Doyle L, Rothlisberger D, Zanghellini A, Gallaher JL, Betker JL, Tanaka F, Barbas CF, III, Hilvert D, Houk KN, Stoddard BL, Baker D. De novo computational design of retro-aldol enzymes. Science 2008;319:1387–1391.
3. Yang W, Jones LM, Isley L, Ye Y, Lee HW, Wilkins A, Liu ZR, Hellinga HW, Malchow R, Ghazi M, Yang JJ. Rational design of a calcium-binding protein. J Am Chem Soc 2003;125:6165–6171.
4. Gohlke H, Klebe G. Approaches to the description and prediction of the binding affinity of small-molecule ligands to macromolecular receptors. Angew Chem Int Ed Engl 2002;41:2644–2676.

5. Karplus M, McCammon JA. Molecular dynamics simulations of biomolecules. Nat Struct Biol 2002;9:646–652.
6. Alexov EG, Gunner MR. Incorporating protein conformational flexibility into the calculation of pH-dependent protein properties. Biophys J 1997;72:2075–2093.
7. Georgescu RE, Alexov EG, Gunner MR. Combining conformational flexibility and continuum electrostatics for calculating pK(a)s in proteins. Biophys J 2002;83:1731–1748.
8. Yang AS, Gunner MR, Sampogna R, Sharp K, Honig B. On the calculation of pK_as in proteins. Proteins 1993;15:252–265.
9. Antosiewicz J, McCammon JA, Gilson MK. Prediction of pH-dependent properties of proteins. J Mol Biol 1994;238:415–436.
10. Nielsen JE, Borchert TV, Vriend G. The determinants of alpha-amylase pH-activity profiles. Protein Eng 2001;14:505–512.
11. Karshikoff A. A simple algorithm for the calculation of multiple site titration curves. Protein Eng 1995;8:243–248.
12. Mehler EL, Guarnieri F. A self-consistent, microenvironment modulated screened coulomb potential approximation to calculate pH-dependent electrostatic effects in proteins. Biophys J 1999;77:3–22.
13. Li H, Robertson AD, Jensen JH. Very fast empirical prediction and rationalization of protein pK(a) values. Proteins 2005;61:704–721.
14. Mongan J, Case DA, McCammon JA. Constant pH molecular dynamics in generalized Born implicit solvent. J Comput Chem 2004;25:2038–2048.
15. Khandogin J, Brooks CL, III. Constant pH molecular dynamics with proton tautomerism. Biophys J 2005;89:141–157.
16. Baptista AM, Martel PJ, Petersen SB. Simulation of protein conformational freedom as a function of pH: constant-pH molecular dynamics using implicit titration. Proteins 1997;27:523–544.
17. Joshi MD, Hedberg A, McIntosh LP. Complete measurement of the pK_a values of the carboxyl and imidazole groups in Bacillus circulans xylanase. Protein Sci 1997;6:2667–2670.
18. Farrell D, Miranda ES, Webb H, Georgi N, Crowley PB, McIntosh LP, Nielsen JE. Titration_DB: Storage and analysis of NMR-monitored protein pH titration curves. Proteins 2010;78:843–857.
19. Toseland CP, McSparron H, Davies MN, Flower DR. PPD v1.0–an integrated, web-accessible database of experimentally determined protein pK_a values. Nucleic Acids Res 2006;34:D199–D203.
20. Grimsley GR, Scholtz JM, Pace CN. A summary of the measured pK values of the ionizable groups in folded proteins. Protein Sci 2009;18:247–251.
21. Forsyth WR, Antosiewicz JM, Robertson AD. Empirical relationships between protein structure and carboxyl pK_a values in proteins. Proteins 2002;48:388–403.
22. Søndergaard CR, McIntosh LP, Pollastri G, Nielsen JE. Determination of electrostatic interaction energies and protonation state populations in enzyme active sites. J Mol Biol 2008;376:269–287.
23. Hass MA, Jensen MR, Led JJ. Probing electric fields in proteins in solution by NMR spectroscopy. Proteins 2008;72:333–343.
24. Sakurai K, Goto Y. Principal component analysis of the pH-dependent conformational transitions of bovine beta-lactoglobulin monitored by heteronuclear NMR. Proc Natl Acad Sci USA 2007;104:15346–15351.
25. Kukic P, Farrell D, Sondergaard CR, Bjarnadottir U, Bradley J, Pollastri G, Nielsen JE. Improving the analysis of NMR spectra tracking pH-induced conformational changes: removing artefacts of the electric field on the NMR chemical shift. Proteins 2010; 78:971–984.
26. Joshi MD, Sidhu G, Pot I, Brayer GD, Withers SG, McIntosh LP. Hydrogen bonding and catalysis: a novel explanation for how a single amino acid substitution can change the pH optimum of a glycosidase. J Mol Biol 2000;299:255–279.
27. Onufriev A, Case DA, Ullmann GM. A novel view of pH titration in biomolecules. Biochemistry 2001;40:3413–3419.
28. Schubert M, Poon DK, Wicki J, Tarling CA, Kwan EM, Nielsen JE, Withers SG, McIntosh LP. Probing electrostatic interactions along the reaction pathway of a glycoside hydrolase: histidine characterization by NMR spectroscopy. Biochemistry 2007;46:7383–7395.
29. Poon DK, Schubert M, Au J, Okon M, Withers SG, McIntosh LP. Unambiguous determination of the ionization state of a glycoside hydrolase active site lysine by 1H-15N heteronuclear correlation spectroscopy. J Am Chem Soc 2006;128:15388–15389.
30. LeMaster DM. Structural determinants of the catalytic reactivity of the buried cysteine of *Escherichia coli* thioredoxin. Biochemistry 1996;35:14876–14881.
31. Markley JL. Observation of histidine residues in proteins by nuclear magnetic resonance spectroscopy. Acc Chem Res 1975;8:70–80.
32. Shrager RI, Cohen JS, Heller SR, Sachs DH, Schechter AN. Mathematical models for interacting groups in nuclear magnetic resonance titration curves. Biochemistry 1972;11:541–547.
33. Farrell D, Georgi N, O'Meara F, Bradley J, Søndergaard CR, Webb H, Tynan-Connolly BM, Bjarnadottir U, Carstensen T, Nielsen JE. Capturing, sharing and analyzing experimental data form protein engineering and directed evolution studies. Nucleic Acids Res 2010. Doi: 10.1093/nar/gkq726.
34. Andre I, Linse S, Mulder FA. Residue-specific pK_a determination of lysine and arginine side chains by indirect 15N and 13C NMR spectroscopy: application to apo calmodulin. J Am Chem Soc 2007; 129:15805–15813.
35. Perez-Canadillas JM, Campos-Olivas R, Lacadena J, Martinez del Pozo A, Gavilanes JG, Santoro J, Rico M, Bruix M. Characterization of pK_a values and titration shifts in the cytotoxic ribonuclease alpha-sarcin by NMR. Relationship between electrostatic interactions, structure, and catalytic function. Biochemistry 1998;37: 15865–15876.
36. Betz M, Lohr F, Wienk H, Ruterjans H. Long-range nature of the interactions between titratable groups in Bacillus agaradhaerens family 11 xylanase: pH titration of *B. agaradhaerens* xylanase. Biochemistry 2004;43:5820–5831.
37. Baran KL, Chimenti MS, Schlessman JL, Fitch CA, Herbst KJ, Garcia-Moreno BE. Electrostatic effects in a network of polar and ionizable groups in staphylococcal nuclease. J Mol Biol 2008;379:1045–1062.
38. Castaneda CA, Fitch CA, Majumdar A, Khangulov V, Schlessman JL, Garcia-Moreno BE. Molecular determinants of the pK_a values of Asp and Glu residues in staphylococcal nuclease. Proteins 2009; 77:570–588.
39. Lee KK, Fitch CA, Lecomte JT, Garcia-Moreno EB. Electrostatic effects in highly charged proteins: salt sensitivity of pK_a values of histidines in staphylococcal nuclease. Biochemistry 2002;41:5656–5667.
40. Bartik K, Redfield C, Dobson CM. Measurement of the individual pK_a values of acidic residues of hen and turkey lysozymes by two-dimensional ^{1}H NMR. Biophys J 1994;66:1180–1184.
41. Kuramitsu S, Hamaguchi K. Analysis of the acid-base titration curve of hen lysozyme. J Biochem (Tokyo). 1980;87:1215–1219.
42. Bradbury JH, Brown LR. Determination of the dissociation constants of the lysine residues of lysozyme by proton-magnetic-resonance spectroscopy. Eur J Biochem 1973;40:565–576.
43. Shindo H, Egan W, et al. Studies of individual carboxyl groups in proteins by carbon 13 nuclear magnetic resonance spectroscopy. J Biol Chem 1978;253:6751–6755.
44. Kuramitsu S, Hamaguchi K. Difference absorption spectra, circular dichroism, and disulfide cleavage of hen and turkey lysozymes in the alkaline pH region. J Biochem 1979;85:443–456.
45. Kuramitsu S, Ikeda K, et al. Participation of the catalytic carboxyls, Asp52 and Glu35, and Asp101 in the binding of substrate analogues to hen lysozyme. J Biochem 1975;77:291–301.
46. Fukae K, Kuramitsu S, et al. Binding of N-acetyl-chitotriose to Asp 52-esterified hen lysozyme. J Biochem 1979;85:141–147.
47. Parsons SM, Raftery MA. Ionization behavior of the catalytic carboxyls of lysozyme. Effects of ionic strength. Biochemistry 1972;11: 1623–1629.
48. Kuramitsu S, Ikeda K, et al. Ionization constants of Glu35 and Asp 52 in hen, turkey, and human lysozymes. J Biochem 1974;76:671–683.

49. Delaglio F, Grzesiek S, Vuister GW, Zhu G, Pfeifer J, Bax A. Nmrpipe—a multidimensional spectral processing system based on unix pipes. J Biomol NMR 1995;6:277–293.
50. Goddard TD, Kneller DG. Sparky 3. San Francisco: University of California, San Francisco.
51. Buck M, Schwalbe H, Dobson CM. Characterization of conformational preferences in a partly folded protein by heteronuclear NMR spectroscopy: assignment and secondary structure analysis of hen egg-white lysozyme in trifluoroethanol. Biochemistry 1995;34: 13219–13232.
52. Yang D, Kay LE. Improved 1HN-detected triple resonance TROSY-based experiments. J Biomol NMR 1999;13:3–10.
53. Wang Y, Bjorndahl TC, Wishart DS. Complete 1H and non-carbonylic 13C assignments of native hen egg-white lysozyme. J Biomol NMR 2000;17:83–84.
54. Schwalbe H, Grimshaw SB, Spencer A, Buck M, Boyd J, Dobson CM, Redfield C, Smith LJ. A refined solution structure of hen lysozyme determined using residual dipolar coupling data. Protein Sci 2001;10:677–688.
55. Oda Y, Yamazaki T, Nagayama K, Kanaya S, Kuroda Y, Nakamura H. Individual ionization constants of all the carboxyl groups in ribonuclease HI from *Escherichia coli* determined by NMR. Biochemistry 1994;33:5275–5284.
56. Yamazaki T, Lee W, Revington M, Mattiello DL, Dahlquist FW, Arrowsmith CH, Kay LE. An Hnca pulse scheme for the backbone assignment of N-15,C-13,H-2-labeled proteins—application to a 37-Kda Trp repressor DNA complex. J Am Chem Soc 1994;116: 6464–6465.
57. Berman HM, Westbrook J, Feng Z, Gilliland G, Bhat TN, Weissig H, Shindyalov IN, Bourne PE. The protein data bank. Nucleic Acids Res 2000;28:235–242.
58. Vriend G. WHAT IF: a molecular modeling and drug design program. J Mol Graph 1990;8:52–56.
59. Nielsen JE, Vriend G. Optimizing the hydrogen-bond network in Poisson-Boltzmann equation-based pK(a) calculations. Proteins 2001; 43:403–412.
60. Nicholls A, Honig B. A rapid finite difference algorithm, utilizing successive over-relaxation to solve the Poisson-Boltzmann equation. J Comp Chem 1991;12:435–445.
61. Rabenstein DL, Sayer TL. Carbon-13 Chemical shift parameters for amines. Carboxylic acids, and amino acids. J Magn Reson 1976; 24:27–39.
62. Surprenant HL, Sarneski JE, Key RR, Byrd JT, Reilley CN. Carbon-13 NMR studies of amino acids: chemical shifts. Protonation shifts microscopic protonation behaviour. J Magn Reson 1980;40:231–243.
63. Tynan-Connolly B, Nielsen JE. pKD: Re-designing protein pK_a values. Nucleic Acids Res 2006;34:W48–W51.
64. Tynan-Connolly BM, Nielsen JE. Re-Designing protein pK_a values. Protein Sci 2007;16:239–249.
65. McIntosh LP, Hand G, Johnson PE, Joshi MD, Korner M, Plesniak LA, Ziser L, Wakarchuk WW, Withers SG. The pK_a of the general acid/base carboxyl group of a glycosidase cycles during catalysis: a 13C-NMR study of bacillus circulans xylanase. Biochemistry 1996;35:9958–9966.
66. Tomlinson JH, Green VL, Baker PJ, Willamson MP. Structural origins of pH-dependent chemical shifts in the B1 domain of protein G. Proteins 2010;78:3000–3016.
67. Chivers PT, Prehoda KE, Volkman BF, Kim BM, Markley JL, Raines RT. Microscopic pK_a values of *Escherichia coli* thioredoxin. Biochemistry 1997;36:14985–14991.
68. Jeng MF, Holmgren A, Dyson HJ. Proton sharing between cysteine thiols in *Escherichia coli* thioredoxin: implications for the mechanism of protein disulfide reduction. Biochemistry 1995;34:10101–10105.
69. Nielsen JE. Analyzing enzymatic pH activity profiles and protein titration curves using structure-based pK_a calculations and titration curve fitting. Methods Enzymol 2009;454:233–258.
70. Davies MN, Toseland CP, Moss DS, Flower DR. Benchmarking pK(a) prediction. BMC Biochem 2006;7:18.
71. Barthelmes J, Ebeling C, Chang A, Schomburg I, Schomburg D. BRENDA. AMENDA and FRENDA: the enzyme information system in 2007. Nucleic Acids Res 2007;35:D511–D514.